
Learning Diffusion at Lightspeed

Antonio Terpin
ETH Zürich
aterpin@ethz.ch

Nicolas Lanzetti
ETH Zürich
lnicolas@ethz.ch

Florian Dörfler
ETH Zürich
dorfler@ethz.ch

Abstract

Diffusion regulates a phenomenal number of natural processes and the dynamics of many successful generative models. Existing models to learn the diffusion terms from observational data rely on complex bilevel optimization problems and properly model only the drift of the system. We propose a new simple model, JKOnet*, which bypasses altogether the complexity of existing architectures while presenting significantly enhanced representational capacity: JKOnet* recovers the potential, interaction, and internal energy components of the underlying diffusion process. JKOnet* minimizes a simple quadratic loss, runs at lightspeed, and drastically outperforms other baselines in practice. Additionally, JKOnet* provides a closed-form optimal solution for linearly parametrized functionals. Our methodology is based on the interpretation of diffusion processes as energy-minimizing trajectories in the probability space via the so-called JKO scheme, which we study via its first-order optimality conditions, in light of few-weeks-old advancements in optimization in the probability space.

1 Introduction

Diffusion processes are omnipresent. They govern the homeostasis of biological systems [36], stem cells reprogramming [16, 32], and the learning dynamics of diffusion models [14, 18, 47] and transformers [15, 45]. The diffusion process of interest often originates from three quantities: a drift term due to a potential, the interaction with other particles, and a stochastic term. If these three components are known, predictions follow from simple forward sampling [23] or the recent work in optimization in the probability space [1, 3, 10, 21, 30, 34, 37]. In this paper, we consider instead the case where the diffusion process is unknown, and we seek to learn its representation from observational data. The problem has been addressed when the trajectories of the individual particles are known [4, 28], but it is often the case that we only have “population data”. For instance, single-cell RNA sequencing techniques enabled the collection of large quantities of data on biological systems [31], but the observer cannot access the trajectories of individual cells since measurements are destructive [16, 32]. The most promising avenue to circumvent the lack of particle trajectories is the Jordan-Kinderlehrer-Otto (JKO) scheme [20] which predicates that the particles as a whole move to decrease an aggregate energy, while not deviating too much from the current configuration. However, the JKO scheme entails an infinite-dimensional optimization problem over the probability space, which poses significant computational challenges. Recent work [1, 8] exploits the theory of optimal transport and in particular Brenier’s theorem [6] to cast the problem as a (challenging) bilevel optimization problem, a model henceforth referred to as JKOnet. Despite promising initial results in [8], this complexity undermines scalability, stability, and generalization capabilities of the model. Furthermore, to be practical, it is limited to learning only potential energies, modelling the underlying physics only partially. Alternatively, [9, 39] learn directly the transport map describing the evolution of the population (i.e., the effects), bypassing the representation of the underlying energy functional (i.e., the causes). Motivated by robustness, interpretability, and generalization, here we seek a method to learn the causes. A similar approach is adopted for instance in [19, 38], where the authors try to

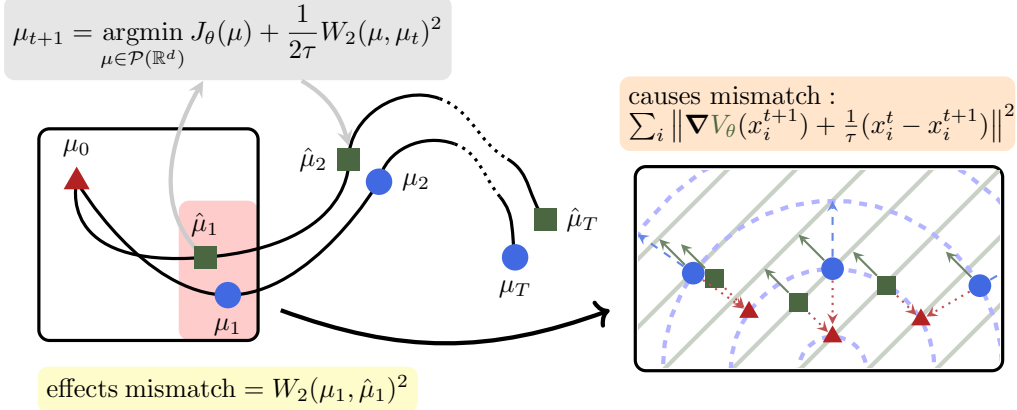


Figure 1: Given a sequence of snapshots (μ_0, \dots, μ_T) of a population of particles undergoing diffusion, we want to find the parameters θ of the parametrized energy function J_θ that best *explains* the particles evolution. Given θ , the **effects mismatch** is the Wasserstein distance between the observed trajectory and the predicted trajectory obtained iteratively solving the **JKO step** with J_θ . In [8], the authors minimize this mismatch differentiating through the resulting bilevel optimization problem. The first-order optimality condition in [26] applied to the JKO step, instead, suggests that the “gradient” of J_θ with respect to each $\hat{\mu}_t$ vanishes at optimality, i.e., for $\hat{\mu}_t = \mu_t$. For $J_\theta(\mu) = \int_{\mathbb{R}^d} V_\theta(x) d\mu(x)$, this condition is depicted on the right. The gradient (dashed blue arrows) of the true V (level curves in dashed blue) at each observed particle x_i^{t+1} (blue circles) in the next snapshot μ_{t+1} opposes the displacement (dotted red arrows) from a particle x_i^t (red triangles) in the previous snapshot μ_t . Instead, the gradient (solid green arrows) of the estimated V_θ (level curves in solid green) at each observed particle x_i^{t+1} (square) does not oppose the displacement from a particle x_i^t in the previous snapshot μ_t . This mismatch in **the causes** of the diffusion process is what JKOnet* minimizes.

learn a geometry that explains the observed transport maps. Unfortunately, the cost between two configurations along a cost-minimizing trajectory is often not a metric [42]. Other attempts include recurrent neural networks [17], neural ODEs [13], and Schrödinger bridges [11, 24]. The latter family of work seeks to recover the velocity field (drift or potential energy) of particles with momentum. In this work, we are interested in diffusion processes (no momentum) and we aim to modeling more general energy functionals. Figure 1 shows an overview of our method, detailed in Section 3.

Contributions We study the first-order necessary optimality conditions for the JKO scheme, an optimization problem in the probability space [26], and show that these conditions can be exploited to learn the energy functional governing the underlying diffusion process from population data, effectively bypassing the complexity of the infinite-dimensional bilevel optimization problem. We provide a closed-form solution in the case of linearly parametrized energy functionals and a simple, interpretable, and efficient algorithm for nonlinear parametrizations. Via exhaustive numerical experiments, we show that, in the case of potential energies only, JKOnet* outperforms the state-of-the-art in terms of solution quality, scalability, and computational efficiency and, in the until now unsolved case of general energy functionals, allows us to also learn interaction and internal energies that explain the observed population trajectories.

2 Diffusion processes via optimal transport

2.1 Preliminaries

The gradient of $\rho : \mathbb{R}^d \rightarrow \mathbb{R}$ is $\nabla \rho \in \mathbb{R}^d$ and the Jacobian of $\phi : \mathbb{R}^d \rightarrow \mathbb{R}^n$ is $\nabla \phi \in \mathbb{R}^{n \times d}$. We say that $f : \mathbb{R}^d \rightarrow \mathbb{R}$ has bounded Hessian if $\|\nabla^2 f(x)\| \leq C$ for some $C > 0$ (and some matrix norm $\|\cdot\|$). The divergence of $F : \mathbb{R}^d \rightarrow \mathbb{R}^n$ is $\nabla \cdot F$ and its laplacian is $\nabla^2 F$. The identity function is $\text{Id} : \mathbb{R}^d \rightarrow \mathbb{R}^d$, $\text{Id}(x) = x$. We denote by $\mathcal{P}(\mathbb{R}^d)$ the space of (Borel) probability

measures over \mathbb{R}^d with finite second moment. For $\mu \in \mathcal{P}(\mathbb{R}^d)$, $\text{supp}(\mu)$ is its support. The Dirac's delta measure at $x \in \mathbb{R}^d$, is δ_x . All the functions are assumed to be Borel, and for $f : \mathbb{R}^d \rightarrow \mathbb{R}$, $\int_{\mathbb{R}^d} f(x) d\mu(x)$ is the (Lebesgue) integral of f w.r.t. μ . If μ is absolutely continuous w.r.t. the Lebesgue measure, $\mu \ll dx$, then it admits a density $\rho : \mathbb{R}^d \rightarrow \mathbb{R}_{\geq 0}$, and the integral becomes $\int_{\mathbb{R}^d} f(x) \rho(x) dx$. The pushforward of μ via a (Borel) map $f : \mathbb{R}^d \rightarrow \mathbb{R}^d$ is the probability measure $f_{\#}\mu$ defined by $(f_{\#}\mu)(B) = \mu(f^{-1}(B))$; when μ is empirical with N , $\mu = \frac{1}{N} \sum_{i=1}^N \delta_{x_i}$, then $f_{\#}\mu = \frac{1}{N} \sum_{i=1}^N \delta_{f(x_i)}$. Given $\mu, \nu \in \mathcal{P}(\mathbb{R}^d)$, we say that a probability measure $\gamma \in \mathcal{P}(\mathbb{R}^d \times \mathbb{R}^d)$ is a transport plan (or coupling) between μ and ν if its marginals are μ and ν . We denote the set of transport plans between μ and ν by $\Gamma(\mu, \nu)$. The Wasserstein distance between μ and ν is

$$W_2(\mu, \nu) := \left(\min_{\gamma \in \Gamma(\mu, \nu)} \int_{\mathbb{R}^d \times \mathbb{R}^d} \|x - y\|^2 d\gamma(x, y) \right)^{\frac{1}{2}}. \quad (1)$$

When μ and ν are discrete, (1) is a linear program. If, additionally, they have the same number of particles, the optimal transport plan is $\gamma = (\text{Id}, T)_{\#}\mu$ for some (transport) map $T : \mathbb{R}^d \rightarrow \mathbb{R}^d$ [35]. When μ is absolutely continuous, $\gamma = (\text{Id}, \nabla\psi)_{\#}\mu$ for some convex function ψ [6].

2.2 The JKO scheme

Many continuous-time diffusion processes can be modeled by partial differential equations (PDEs) or stochastic differential equations (SDEs):

Example 2.1 (Fokker-Planck). *The Fokker-Planck equation,*

$$\frac{\partial \rho_t}{\partial t} = \nabla \cdot (\nabla V \rho_t) + \beta \nabla^2 \rho_t, \quad (2)$$

describes the time evolution of the distribution of a set of particles undergoing drift and diffusion,

$$dX(t) = -\nabla V(X(t))dt + \sqrt{2\beta}dW(t),$$

where $X(t)$ is the state of the particle, $V(x)$ the potential causing the drift, and $W(t)$ the standard Wiener process.

The pioneering work of Jordan, Kinderlehrer, and Otto [20], related diffusion processes to energy-minimizing trajectories in the Wasserstein space (i.e., probability space endowed with the Wasserstein distance). This modern perspective provides us with a natural discrete-time counterpart of the diffusion process, the JKO scheme,

$$\mu_{t+1} = \underset{\mu \in \mathcal{P}(\mathbb{R}^d)}{\text{argmin}} J(\mu) + \frac{1}{2\tau} W_2(\mu, \mu_t)^2, \quad (3)$$

where $J : \mathcal{P}(\mathbb{R}^d) \rightarrow \mathbb{R} \cup \{+\infty\}$ is an energy functional and $\tau > 0$ is the time discretization.

Example 2.2 (Fokker-Planck as a Wasserstein gradient flow). *The Fokker-Planck equation (2) results from the continuous-time limit (i.e., $\tau \rightarrow 0$) of the JKO scheme (3) for the energy functional*

$$J(\mu) = \int_{\mathbb{R}^d} V(x) d\mu(x) + \beta \int_{\mathbb{R}^d} \rho(x) \log(\rho(x)) dx \quad \text{with} \quad d\mu(x) = \rho(x) dx.$$

2.3 Challenges

Section 2.2 suggests that we can interpret the problem of learning diffusion processes as the problem of learning the energy functional J in (3). Specifically, the setting is as follows: We have access to sample populations $\mu_0, \mu_1, \dots, \mu_T$, and we want to learn the energy functional governing their dynamics. A direct approach to tackle the inverse problem is a bilevel optimization, used, among others, for the model JKOnet in [8]. This approach bases on the following two facts. First, by Brenier's theorem, the solution of (3), μ_{t+1} , can be expressed¹ as the pushforward of μ_t via the gradient of a convex function $\psi_t : \mathbb{R}^d \rightarrow \mathbb{R}$ and, thus,

$$W_2(\mu_t, \mu_{t+1})^2 = \int_{\mathbb{R}^d} \|x - \nabla\psi_t(x)\|^2 d\mu_t(x).$$

¹Under an absolute continuity assumption.

Second, the optimization problem (3) is equivalently written as

$$\operatorname{argmin}_{\psi_t \in C} J(\nabla\psi_t \# \mu_t) + \frac{1}{2\tau} \int_{\mathbb{R}^d} \|x - \nabla\psi_t(x)\|^2 d\mu_t(x),$$

where C is the class of continuously differentiable convex functions from \mathbb{R}^d to \mathbb{R} . Therefore, the learning task can be cast into the following bilevel optimization problem, which minimizes the discrepancy between the observations (μ_t) and the predictions of the model ($\hat{\mu}_t$):

$$\begin{aligned} \min_J \sum_{t=1}^T W_2(\hat{\mu}_t, \mu_t)^2 \\ \text{s.t. } \hat{\mu}_0 = \mu_0, \quad \hat{\mu}_{t+1} = \nabla\psi_t^* \hat{\mu}_t, \\ \psi_t^* := \operatorname{argmin}_{\psi \in C} J(\nabla\psi \# \hat{\mu}_t) + \frac{1}{2\tau} \int_{\mathbb{R}^d} \|x - \nabla\psi(x)\|^2 d\hat{\mu}_t(x). \end{aligned} \quad (4)$$

A practical implementation of the above requires a parametrization of both the transport map and the energy functional. The former problem has been tackled via input convex neural network (ICNN) parametrizing ψ_t [2, 7] or via the ‘‘Monge gap’’ [44]. The second problem is only addressed for energy functional of the form $J(\mu) = \int_{\mathbb{R}} V_\theta(x) d\mu(x)$, without interaction and internal energies, where V_θ is a non-linear function approximator [8].

Challenges. This approach suffers from two major limitations. First, bilevel optimization problems are notoriously hard and we should therefore expect (4) to be computationally challenging. Second, most energy functionals are not potential energies but include interactions and internal energy terms as well. Although it is tempting to include other terms in the energy functional J (e.g., parametrizing interaction and internal energies), the complexity of the bilevel optimization problem renders such an avenue viable only in principle.

3 Learning diffusion at lightspeed

Our methodology consists of replacing the optimization problem (3) with its first-order necessary conditions for optimality. This way, we bypass its computational complexity which, ultimately, leads to the bilevel optimization problem (4). Perhaps interestingly, our methodology for learning diffusion is based on first principles: whereas e.g. [8] minimizes an error on the *effects* (the predictions), we minimize an error on the *causes* (the energy functionals driving the diffusion process); see Figure 1. As we detail in Section 4, the resulting learning algorithms are significantly faster and more effective.

3.1 Intuition

To start, we illustrate our idea in the Euclidean case (i.e., \mathbb{R}^d) and later show that it readily generalizes to the probability space (i.e., $\mathcal{P}(\mathbb{R}^d)$). Consider the problem of learning the energy functional $J : \mathbb{R}^d \rightarrow \mathbb{R} \cup \{+\infty\}$ of a dynamics resulting from the analog of the JKO scheme in the Euclidean space, the proximal operator

$$x_{t+1} = \operatorname{argmin}_{x \in \mathbb{R}^d} J(x) + \frac{1}{2\tau} \|x - x_t\|^2. \quad (5)$$

Under sufficient regularity, we can replace (5) by its first-order optimality condition

$$\nabla J(x_{t+1}) + \frac{1}{\tau}(x_{t+1} - x_t) = 0. \quad (6)$$

Given a dataset (x_0, x_1, \dots, x_T) , we seek the energy functional that best fits the optimality condition:

$$\min_J \sum_{t=0}^{T-1} \left\| \nabla J(x_{t+1}) + \frac{1}{\tau}(x_{t+1} - x_t) \right\|^2. \quad (7)$$

In the probability space, we can proceed analogously and replace (3) with its first-order optimality conditions. This analysis, which is based on recent advancements in optimization in the probability space [26], allows us to formulate the learning task as a single-level optimization problem.

3.2 Potential energy

Consider initially the case where the energy functional is a potential energy, for $V : \mathbb{R}^d \rightarrow \mathbb{R}$,

$$J(\mu) = \int_{\mathbb{R}^d} V(x) d\mu(x). \quad (8)$$

The following proposition is the counterpart of (6) in $\mathcal{P}(\mathbb{R}^d)$:

Proposition 3.1 (Potential energy). *Assume V is continuously differentiable, lower bounded, and has a bounded Hessian. Then, the JKO scheme (3) has an optimal solution μ_{t+1} and, if μ_{t+1} is optimal for (3), then there is an optimal transport plan γ_t between μ_t and μ_{t+1} such that*

$$\int_{\mathbb{R}^d \times \mathbb{R}^d} \left\| \nabla V(x_{t+1}) + \frac{1}{\tau}(x_{t+1} - x_t) \right\|^2 d\gamma_t(x_t, x_{t+1}) = 0.$$

Proposition 3.1 is by all means the analog of (6), since for the integral to be zero, $\nabla V(x_{t+1}) + \frac{1}{\tau}(x_{t+1} - x_t) = 0$ must hold for all $(x_t, x_{t+1}) \in \text{supp}(\gamma_t)$. Since the collected population data $\mu_0, \mu_1, \dots, \mu_T$ are not optimization variables in the learning task, the optimal transport plan γ_t can be computed beforehand. Thus, we can learn the energy functional representation by minimizing over a class of continuously differentiable potential energy functions the loss function

$$\sum_{t=0}^{T-1} \int_{\mathbb{R}^d \times \mathbb{R}^d} \left\| \nabla V(x_{t+1}) + \frac{1}{\tau}(x_{t+1} - x_t) \right\|^2 d\gamma_t(x_t, x_{t+1}). \quad (9)$$

3.3 Arbitrary energy functionals

Consider now the general case where the energy functional consists of a potential energy (with the potential function $V : \mathbb{R}^d \rightarrow \mathbb{R}$), interaction energy (with interaction kernel $U : \mathbb{R}^d \rightarrow \mathbb{R}$), and internal energy (expressed as the entropy weighted by $\beta \in \mathbb{R}_{\geq 0}$):

$$J(\mu) = \int_{\mathbb{R}^d} V(x) d\mu(x) + \int_{\mathbb{R}^d \times \mathbb{R}^d} U(x-y) d(\mu \times \mu)(x, y) + \beta \int_{\mathbb{R}^d} \rho(x) \log(\rho(x)) dx. \quad (10)$$

The first-order necessary optimality condition for the JKO scheme then reads as follows.

Proposition 3.2 (General case). *Assume V and U are continuously differentiable, lower bounded, and have a bounded Hessian. Then, the JKO scheme (3) has an optimal solution μ_{t+1} which is absolutely continuous with density ρ_{t+1} and, if $d\mu_{t+1}(x) = \rho_{t+1}(x) dx$ is optimal for (3), then there is an optimal transport plan γ_t between μ_t and μ_{t+1} such that*

$$0 = \int_{\mathbb{R}^d \times \mathbb{R}^d} \left\| \nabla V(x_{t+1}) + \int_{\mathbb{R}^d} \nabla U(x_{t+1} - x'_{t+1}) d\mu_{t+1}(x'_{t+1}) + \beta \frac{\nabla \rho_{t+1}(x_{t+1})}{\rho_{t+1}(x_{t+1})} + \frac{1}{\tau}(x_{t+1} - x_t) \right\|^2 d\gamma_t(x_t, x_{t+1}).$$

Thus, Proposition 3.2 suggests that the energy functional can be learned by minimizing over a class of continuously differentiable potential and internal energy functions and $\beta \in \mathbb{R}_{\geq 0}$ the loss function

$$\sum_{t=0}^{T-1} \int_{\mathbb{R}^d \times \mathbb{R}^d} \left\| \nabla V(x_{t+1}) + \int_{\mathbb{R}^d} \nabla U(x_{t+1} - x'_{t+1}) d\mu_{t+1}(x'_{t+1}) + \beta \frac{\nabla \rho_{t+1}(x_{t+1})}{\rho_{t+1}(x_{t+1})} + \frac{1}{\tau}(x_{t+1} - x_t) \right\|^2 d\gamma_t(x_t, x_{t+1}). \quad (11)$$

Remark 3.3. Our formulation readily generalizes to time-varying energies.

3.4 Parametrizations

For our model JKOnet*, we parametrize the energy functional at a measure $d\mu = \rho(x) dx$ as follows:

$$J_\theta(\mu) = \int_{\mathbb{R}^d} V_{\theta_1}(x) d\mu(x) + \int_{\mathbb{R}^d \times \mathbb{R}^d} U_{\theta_2}(x-y) d(\mu \times \mu)(x, y) + \theta_3 \int_{\mathbb{R}^d} \rho(x) \log(\rho(x)) dx,$$

where $\theta_1, \theta_2 \in \mathbb{R}^n, \theta_3 \in \mathbb{R}$, and we set $\theta = [\theta_1^\top, \theta_2^\top, \theta_3^\top]^\top \in \mathbb{R}^{2n+1}$.

| Model | FLOPS per training step | Seq. op. per particle | Generality | | |
|------------------------------------|---|---|------------|---------|--------|
| | | | $V(x)$ | β | $U(x)$ |
| JK0net w/o TF | $\mathcal{O}\left(T\left(DNd + \frac{N^2 \log(N)}{\varepsilon^2}\right)\right)$ | $\mathcal{O}\left(T\left(DNd + \frac{N^2 \log(N)}{\varepsilon^2}\right)\right)$ | ✓ | × | × |
| JK0net w/ TF | $\mathcal{O}\left(T\left(DNd + \frac{N^2 \log(N)}{\varepsilon^2}\right)\right)$ | $\mathcal{O}\left(DNd + \frac{N^2 \log(N)}{\varepsilon^2}\right)$ | ✓ | × | × |
| JK0net w/ MG w/o TF | $\mathcal{O}\left(TD\left(Nd + \frac{N^2 \log(N)}{\varepsilon^2}\right)\right)$ | $\mathcal{O}\left(TD\left(Nd + \frac{N^2 \log(N)}{\varepsilon^2}\right)\right)$ | ✓ | × | × |
| JK0net w/ MG, TF | $\mathcal{O}\left(TD\left(Nd + \frac{N^2 \log(N)}{\varepsilon^2}\right)\right)$ | $\mathcal{O}\left(D\left(Nd + \frac{N^2 \log(N)}{\varepsilon^2}\right)\right)$ | ✓ | × | × |
| JK0net* w/o $U(x)$ | $\mathcal{O}(TNd)$ | $\mathcal{O}(d)$ | ✓ | ✓ | × |
| JK0net* w/ $U(x)$ | $\mathcal{O}(TN^2d)$ | $\mathcal{O}(Nd)$ | ✓ | ✓ | ✓ |
| JK0net* _t w/o $U(x)$ | $\mathcal{O}(TNdn + n^3)$ | $\mathcal{O}(TNdn + n^3)$ | ✓ | ✓ | × |
| JK0net* _t w/ $U(x)$ | $\mathcal{O}(TN^2dn + n^3)$ | $\mathcal{O}(TN^2dn + n^3)$ | ✓ | ✓ | ✓ |

Table 1: Per-epoch complexity (in FLOPs) and per-particle minimum number of sequential operations (maximum parallelization) for the JK0net and JK0net* model families. Here, T is the length of the population trajectory, N the number of particles in the snapshots of the population (assumed constant), d is the dimensionality of the system, n is the number of features for the linear parametrization, D, ε , TeacherForcing (TF) are JK0net parameters: the number of inner operations (which may or not be constant), the accuracy required for the Sinkhorn algorithm, and a training modality (see [8] for details), respectively. MG stands for the Monge gap regularization [44].

Linear parametrizations. When the parametrizations are linear, i.e. $V_{\theta_1}(x) = \theta_1^\top \phi(x)$, $U_{\theta_2}(x - y) = \theta_2^\top \phi(x - y)$ for feature maps $\phi_1, \phi_2 : \mathbb{R}^d \rightarrow \mathbb{R}^n$, the optimal θ^* can be computed in closed-form:

Proposition 3.4. Assume that the features $\phi_{1,i}$ and $\phi_{2,i}$ are continuously differentiable, bounded, and have bounded Hessian. Define the matrix $y_t : \mathbb{R}^d \rightarrow \mathbb{R}^{(2n+1) \times d}$ by

$$y_t(x_t) := \left[\nabla \phi_1(x_t)^\top, \int_{\mathbb{R}^d} \nabla \phi_2(x_t - x'_t)^\top d\mu_t(x'_t), \frac{\nabla \rho_t(x_t)}{\rho_t(x_t)} \right]^\top$$

and suppose that the data is sufficiently exciting so that $\sum_{t=1}^T \int_{\mathbb{R}^d} y_t(x_t) y_t(x_t)^\top d\mu_t(x_t)$ is invertible. Then, the optimal solution of (11) is

$$\theta^* = \frac{1}{\tau} \left(\sum_{t=1}^T \int_{\mathbb{R}^d} y_t(x_t) y_t(x_t)^\top d\mu_t(x_t) \right)^{-1} \left(\sum_{t=0}^{T-1} \int_{\mathbb{R}^d \times \mathbb{R}^d} y_t(x_{t+1})(x_{t+1} - x_t) d\gamma_t(x_t, x_{t+1}) \right). \quad (12)$$

Remark 3.5. The excitation assumption can be enforced via regularization terms $\lambda_i \|\theta_i\|^2$, with $\lambda_i > 0$, in the loss (11). Another practical alternative is to use pseudoinverse or solve the least-squares problem corresponding to (12) by gradient descent.

Non-linear parametrizations. When the parametrizations are non-linear, we minimize (11) by gradient descent.

Inductive biases. By fixing any of the parameters $\theta_1, \theta_2, \theta_3$ to zero, the corresponding energy term is dropped from the model. It is thus possible to inject into JK0net* the proper inductive bias when additional information on the underlying diffusion process are known. For instance, if the process is deterministic and driven by an external potential, one can set $\theta_2 = \theta_3 = 0$. Similarly, if it can be assumed that the interaction between the particles is negligible, we can set $\theta_2 = 0$.

3.5 Why first-order conditions

Here, we motivate the theoretical benefits of JK0net* over JK0net using the desiderata:

1. Total computational complexity per epoch (i.e., the cost to process the observed populations).
2. Per-particle computational complexity (i.e., the cost to process a single particle when maximally parallelizing the algorithm, prior to merging the results).
3. Representational capacity of the method (i.e., which energy terms the model can learn).

We collect this analysis in Table 1. Fundamentally, the first-order optimality conditions allow a reformulation of the learning problem that decouples prediction of the population evolution and learning of the dynamics (such coupling is the crux of (4)). As a result, JK0net* enjoys higher parallelizability. We also observe that the interaction energy comes with an increase in complexity, and in a way resembles the attention mechanisms in transformers [45, 15]. The linear dependence of JK0net* on the size of the batch implies that our method can process larger batch sizes for free (to process the entire dataset we need fewer steps in an inverse relationship with the batch size). In practice, this actually increases the speed (less memory swaps). These considerations do not hold for the JK0net family. Finally, JK0net* enjoys enhanced representational power and interpretability. JK0net_l* generally needs more computation per epoch (primarily related to the number of features) but requires a single epoch. In Table 1 we also report the computational complexity of the variants of JK0net using a vanilla multi-layer perceptron (MLP) with Monge gap regularization [44] instead of a ICNN as a parametrization of the transport map. Despite the success in simplifying the training of transport maps over the use of ICNN [44], the Monge gap requires the solution of an optimal transport problem at every inner iteration, an unbearable slowdown [29].

4 Experiments

We assess the ability of JK0net* to learn diffusion processes in various settings. The code is available at <https://github.com/antonioterpin/jkonet-star>. We include the training and architectural details for the JK0net* models family in Appendix C. The settings of the baselines considered are the one provided by the corresponding papers, reported for completeness in Appendix E, and the hardware setup is described in Appendix C.7. In all the experiments, we allow the models a budget of 1000 epochs.

Our models. We use the following terminology for our method. JK0net* is the most general non-linear parametrization in Section 3.4 and JK0net_v* introduces the inductive bias $\theta_2 = \theta_3 = 0$. Similarly, we refer to the linear parametrizations by JK0net_{l,v}* and JK0net_l*.

Metrics. To evaluate the overall prediction capabilities, instead, we consider the cumulative square Wasserstein distance over the trajectory, i.e., $\sum_{t=1}^T W_2(\mu_t, \hat{\mu}_t)^2$, where μ_t and $\hat{\mu}_t$ are the observed and predicted populations, respectively.

4.1 Training at lightspeed

Experimental setting. We validate the observations in Section 3.5 comparing (i) the Wasserstein error and (ii) the time per epoch required by the different methods on a synthetic dataset consisting of particles subject to a non-linear drift (potential energy minimization only, see Appendix F).

Results. Figure 3 summarizes our results. All our methods perform uniformly better than the baseline, regardless of the generality. The speed improvement of the JK0net* models family suggests that a theoretically guided loss may provide strong computational benefits on par to sophisticated model architectures. In fact, while each experiment (in this and other sections) takes only a few minutes for the JK0net* models, it can take several hours for the JK0net family. Note also that JK0net_l* and JK0net_{l,v}* require a computational time per epoch comparable to the JK0net family, but they only need one epoch to solve the problem optimally. The true and estimated level curves of the potentials, as well as the predicted evolutions, are depicted in Figure 2 and Figure 5.

Remarkably, the increase in expressivity and efficiency of the model does not require a more complex architecture. Compared to JK0net (cf. [8]), we drop the additional ICNN used in the inner iteration and the related training details (e.g., the strong convexity regularizer and the teacher forcing). Simply replacing the ICNN in JK0net deprives the method of the theoretical connections with optimal transport, and in our experiments this appears to be associated with stability (NaN in Figure 3).

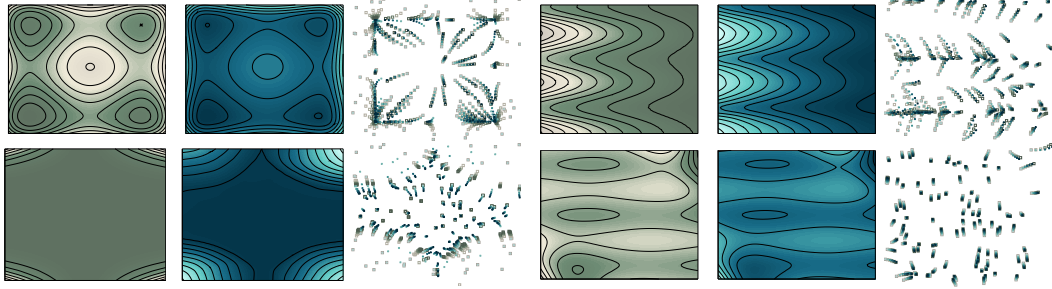


Figure 2: Level curves of the true (green-colored) and estimated (blue-colored) potentials (27), (33), (37) and (32). The third plot of each group depicts the observed (empty green squares) and predicted (blue crosses) particles evolution. See also Figure 5.

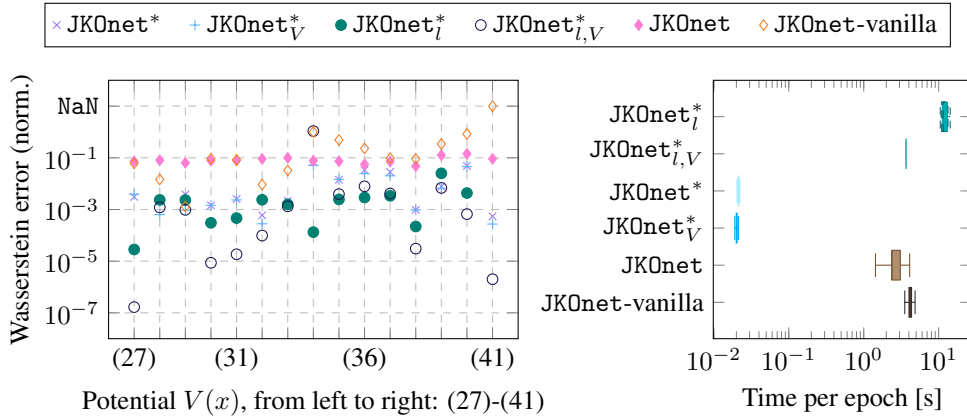


Figure 3: Numerical results of Section 4.1. The scatter plot displays points (x_i, y_i) where x_i indexes the potentials in Appendix F and y_i are the errors obtained with the different models. We mark with NaN each method that has diverged during training. The box plot analyses the time per epoch required by each method. The statistics are across all the epochs and all the potential energies.

4.2 Scaling laws

Experimental setting. Enabled by the computational efficiency of JK0net^{*2}, we run an ablation study on the number of dimensions and on the size of the dataset. Specifically, we assess the performances of JK0net^{*}_V to recover the correct potential energy given $N \in \{1000, 2500, 5000, 7500, 10000\}$ particles in dimension $d \in \{10, 20, 30, 40, 50\}$.

Results. We summarize our findings in Figure 4 for the potentials (27), (30), and (32) in Appendix F, and for all the potentials in Figure 6. In particular, JK0net^{*}_l keeps a stable color along the rows, which suggests an almost constant error (the Wasserstein error is related to a quadratic norm and, thus, is expected to have a linear growth with the dimension d ; here, the growth is strongly sublinear) up to the point where the number of particles is not informative enough (along the columns, the error indeed decreases again). We thus conclude that JK0net^{*} is well suited for high-dimensional tasks.

4.3 General Energy Functionals

Experimental setting. We showcase the capabilities of the JK0net^{*} models to recover the potential, interaction, and internal energies selected as combinations of the functions in Appendix F and noise levels $\beta \in \{0.0, 0.1, 0.2\}$. To the best of our knowledge, ours is the first model capable of recovering all three energy terms.

²The computational demand of JK0net, apparent in Figure 3, prevented us from exploring the scaling laws of the method.

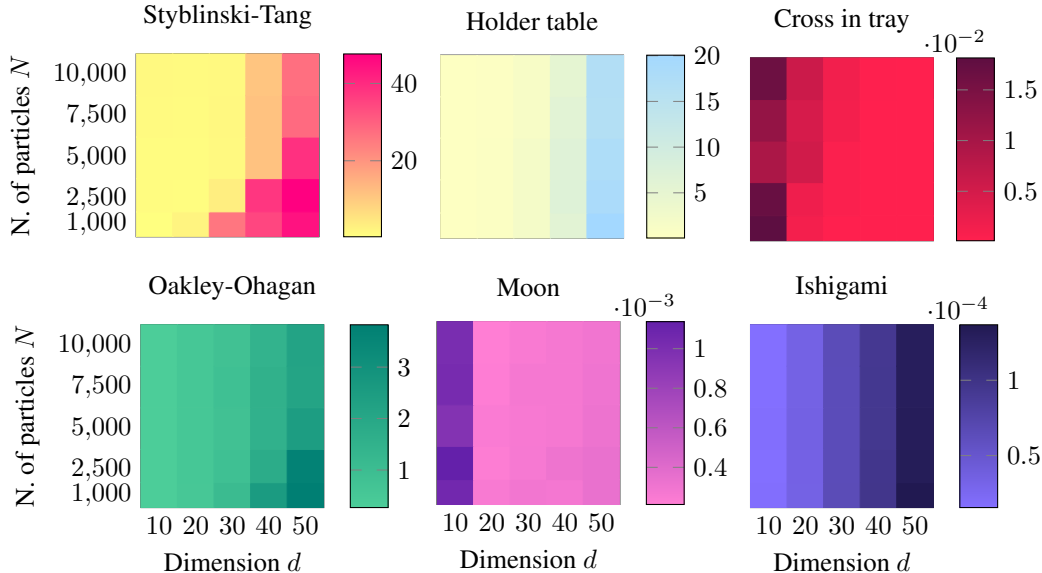
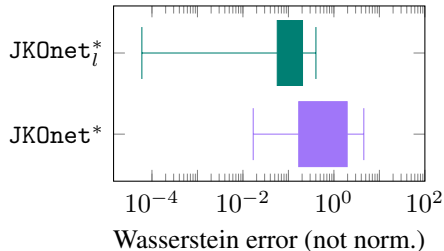


Figure 4: Numerical results of Section 4.2, reported in full in Figure 6. The colors of each cell represent the Wasserstein error. Thus, a method that scales well to high-dimensional settings should display a relatively stable color along the rows (the error is related to the norm and, thus, is linear in the dimension d ; here, the growth is sublinear).

Results. We summarize our findings on the right³. Compared to the setting in Section 4.1, there are two additional sources of inaccuracies: (i) the effect of noise, which introduces an inevitable sampling error, and the (ii) the approximations in the estimation of the densities (e.g., Propositions 3.2 and 3.4, and Appendix C for training details). Nonetheless, the low Wasserstein errors demonstrate the capability of our method to correctly recover potential, interaction, and internal energies that best explain the observed populations.



5 Conclusion and limitations

Contributions. We introduced JK0net*, a model which recovers the energy functionals governing various classes of diffusion processes. The model bases on the novel study of the first-order optimality conditions of the JKO scheme, which drastically simplifies the learning task. In particular, we replace the complex bilevel optimization problem with a simple mean-square error, outperforming the baseline in terms of computational requirements, accuracy, and expressiveness.

Limitations. Our work did not address a few important challenges, which we believe to be exciting open questions. On the practical side, JK0net* owns its performances to a loss function motivated by deep theoretical results. However, its architecture is still “vanilla” and we did not investigate data domains like images. Moreover, this work does not investigate in detail the choice of features for the linear parametrization, which in our experiments displays extremely promising results nonetheless.

Outlook. We expect the approach followed in this work to similarly apply to other exciting avenues of applied machine learning research, such as population steering [42], reinforcement learning [33, 40, 43], diffusion models [14, 18, 47] and transformers [15, 45].

³Some of these experiments ($\sim 8\%$) failed due to numerical instabilities, mainly due to the fitting of Gaussian mixtures (see Appendix C.3 for details), for a total of reported experiments of 497.

References

- [1] David Alvarez-Melis, Yair Schiff, and Youssef Mroueh. Optimizing functionals on the space of probabilities with input convex neural networks. *Transactions on Machine Learning Research*, 2022.
- [2] Brandon Amos, Lei Xu, and J Zico Kolter. Input convex neural networks. In *International Conference on Machine Learning*, pages 146–155. PMLR, 2017.
- [3] Jean-David Benamou, Guillaume Carlier, and Maxime Laborde. An augmented lagrangian approach to Wasserstein gradient flows and applications. *ESAIM: Proceedings and surveys*, 54:1–17, 2016.
- [4] Riccardo Bonalli and Alessandro Rudi. Non-parametric learning of stochastic differential equations with fast rates of convergence. *arXiv preprint arXiv:2305.15557*, 2023.
- [5] James Bradbury, Roy Frostig, Peter Hawkins, Matthew James Johnson, Chris Leary, Dougal Maclaurin, George Necula, Adam Paszke, Jake VanderPlas, Skye Wanderman-Milne, and Qiao Zhang. JAX: composable transformations of Python+NumPy programs, 2018.
- [6] Yann Brenier. Polar factorization and monotone rearrangement of vector-valued functions. *Communications on Pure and Applied Mathematics*, 44(4):375–417, 1991.
- [7] Charlotte Bunne, Andreas Krause, and Marco Cuturi. Supervised training of conditional monge maps. *Advances in Neural Information Processing Systems*, 35:6859–6872, 2022.
- [8] Charlotte Bunne, Laetitia Meng-Papaxanthos, Andreas Krause, and Marco Cuturi. Proximal optimal transport modeling of population dynamics. In *International Conference on Artificial Intelligence and Statistics (AISTATS)*, 2022.
- [9] Charlotte Bunne, Stefan G Stark, Gabriele Gut, Jacobo Sarabia Del Castillo, Mitch Levesque, Kjong-Van Lehmann, Lucas Pelkmans, Andreas Krause, and Gunnar Rätsch. Learning single-cell perturbation responses using neural optimal transport. *Nature Methods*, pages 1–10, 2023.
- [10] José A Carrillo, Katy Craig, Li Wang, and Chaozhen Wei. Primal dual methods for Wasserstein gradient flows. *Foundations of Computational Mathematics*, pages 1–55, 2022.
- [11] Tianrong Chen, Guan-Horng Liu, Molei Tao, and Evangelos A Theodorou. Deep momentum multi-marginal schrödinger bridge. *arXiv preprint arXiv:2303.01751*, 2023.
- [12] Marco Cuturi, Laetitia Meng-Papaxanthos, Yingtao Tian, Charlotte Bunne, Geoff Davis, and Olivier Teboul. Optimal transport tools (ott): A JAX toolbox for all things Wasserstein. *arXiv preprint arXiv:2201.12324*, 2022.
- [13] Rossin Erbe, Genevieve Stein-O’Brien, and Elana J Fertig. Transcriptomic forecasting with neural ordinary differential equations. *Patterns*, 4(8), 2023.
- [14] Patrick Esser, Sumith Kulal, Andreas Blattmann, Rahim Entezari, Jonas Müller, Harry Saini, Yam Levi, Dominik Lorenz, Axel Sauer, Frederic Boesel, Dustin Podell, Tim Dockhorn, Zion English, Kyle Lacey, Alex Goodwin, Yannik Marek, and Robin Rombach. Scaling rectified flow transformers for high-resolution image synthesis. *arXiv preprint arXiv:2403.03206*, 2024.
- [15] Borjan Geshkovski, Cyril Letrouit, Yury Polyanskiy, and Philippe Rigollet. A mathematical perspective on transformers. *arXiv preprint arXiv:2312.10794*, 2023.
- [16] Jacob Hanna, Krishanu Saha, Bernardo Pando, Jeroen Van Zon, Christopher J Lengner, Menno P Creyghton, Alexander van Oudenaarden, and Rudolf Jaenisch. Direct cell reprogramming is a stochastic process amenable to acceleration. *Nature*, 462(7273):595–601, 2009.
- [17] Tatsunori Hashimoto, David Gifford, and Tommi Jaakkola. Learning population-level diffusions with generative rnns. In *International Conference on Machine Learning*, pages 2417–2426. PMLR, 2016.
- [18] Jonathan Ho, Ajay Jain, and Pieter Abbeel. Denoising diffusion probabilistic models. *arXiv preprint arXiv:2006.11239*, 2020.
- [19] Guillaume Huguet, Daniel Sumner Magruder, Alexander Tong, Oluwadamilola Fasina, Manik Kuchroo, Guy Wolf, and Smita Krishnaswamy. Manifold interpolating optimal-transport flows for trajectory inference. *Advances in Neural Information Processing Systems*, 35:29705–29718, 2022.

- [20] Richard Jordan, David Kinderlehrer, and Felix Otto. The variational formulation of the fokker-planck equation. *SIAM journal on mathematical analysis*, 29(1):1–17, 1998.
- [21] Carson Kent, Jiajin Li, Jose Blanchet, and Peter W Glynn. Modified frank wolfe in probability space. In *Advances in Neural Information Processing Systems*, volume 34, pages 14448–14462. Curran Associates, Inc., 2021.
- [22] Diederik P. Kingma and Jimmy Ba. Adam: A method for stochastic optimization. In Yoshua Bengio and Yann LeCun, editors, *3rd International Conference on Learning Representations, ICLR 2015, San Diego, CA, USA, May 7-9, 2015, Conference Track Proceedings*, 2015.
- [23] Peter E Kloeden, Eckhard Platen, Peter E Kloeden, and Eckhard Platen. *Stochastic differential equations*. Springer, 1992.
- [24] Takeshi Koshizuka and Issei Sato. Neural lagrangian schrödinger bridge: Diffusion modeling for population dynamics. In *The Eleventh International Conference on Learning Representations*, 2022.
- [25] Nicolas Lanzetti, Saverio Bolognani, and Florian Dörfler. First-order conditions for optimization in the Wasserstein space. *arXiv preprint arXiv:2209.12197*, 2022.
- [26] Nicolas Lanzetti, Antonio Terpin, and Florian Dörfler. Variational analysis in the wasserstein space. *arXiv preprint arXiv:2406.10676*, 2024.
- [27] Juho Lee, Yoonho Lee, Jungtaek Kim, Adam R. Kosiosek, Seungjin Choi, and Yee Whye Teh. Set transformer: A framework for attention-based permutation-invariant neural networks. *arXiv preprint arXiv:1810.00825*, 2019.
- [28] Xuechen Li, Ting-Kam Leonard Wong, Ricky TQ Chen, and David Duvenaud. Scalable gradients for stochastic differential equations. In *International Conference on Artificial Intelligence and Statistics*, pages 3870–3882. PMLR, 2020.
- [29] Jianzhou Luo, Dingchuan Yang, and Ke Wei. Improved complexity analysis of the sinkhorn and greenhorn algorithms for optimal transport. *arXiv preprint arXiv:2305.14939*, 2023.
- [30] Petr Mokrov, Alexander Korotin, Lingxiao Li, Aude Genevay, Justin M Solomon, and Evgeny Burnaev. Large-scale wasserstein gradient flows. *Advances in Neural Information Processing Systems*, 34:15243–15256, 2021.
- [31] Kevin R Moon, David van Dijk, Zheng Wang, Scott Gigante, Daniel B Burkhardt, William S Chen, Kristina Yim, Antonia van den Elzen, Matthew J Hirn, Ronald R Coifman, et al. Visualizing structure and transitions in high-dimensional biological data. *Nature biotechnology*, 37(12):1482–1492, 2019.
- [32] Rob Morris, Ignacio Sancho-Martinez, Tatyana O Sharpee, and Juan Carlos Izpisua Belmonte. Mathematical approaches to modeling development and reprogramming. *Proceedings of the National Academy of Sciences*, 111(14):5076–5082, 2014.
- [33] Mirco Mutti, Riccardo De Santi, Piersilvio De Bartolomeis, and Marcello Restelli. Challenging common assumptions in convex reinforcement learning. *Advances in Neural Information Processing Systems*, 35:4489–4502, 2022.
- [34] Gabriel Peyré. Entropic approximation of Wasserstein gradient flows. *SIAM Journal on Imaging Sciences*, 8(4):2323–2351, 2015.
- [35] Gabriel Peyré and Marco Cuturi. Computational optimal transport. *arXiv preprint arXiv:1803.00567*, 2020.
- [36] Jane B Reece, Lisa A Urry, and Michael L Cain. *Campbell biology*. Pearson, 2017.
- [37] Filippo Santambrogio. Optimal transport for applied mathematicians. *Birkhäuser, NY*, 55(58-63):94, 2015.
- [38] Christopher Scovel and Justin Solomon. Riemannian metric learning via optimal transport. *arXiv preprint arXiv:2205.09244*, 2022.
- [39] Geoffrey Schiebinger, Jian Shu, Marcin Tabaka, Brian Cleary, Vidya Subramanian, Aryeh Solomon, Joshua Gould, Siyan Liu, Stacie Lin, Peter Berube, et al. Optimal-transport analysis of single-cell gene expression identifies developmental trajectories in reprogramming. *Cell*, 176(4):928–943, 2019.
- [40] John Schulman, Filip Wolski, Prafulla Dhariwal, Alec Radford, and Oleg Klimov. Proximal policy optimization algorithms. *arXiv preprint arXiv:1707.06347*, 2017.

- [41] Simon Fraser University. Test functions and datasets for optimization, 2023. Accessed: 2024-05-15.
- [42] Antonio Terpin, Nicolas Lanzetti, and Florian Dörfler. Dynamic programming in probability spaces via optimal transport. *SIAM Journal on Control and Optimization*, 62(2):1183–1206, 2024.
- [43] Antonio Terpin, Nicolas Lanzetti, Batuhan Yardim, Florian Dorfler, and Giorgia Ramponi. Trust region policy optimization with optimal transport discrepancies: Duality and algorithm for continuous actions. *Advances in Neural Information Processing Systems*, 35:19786–19797, 2022.
- [44] Théo Uscidda and Marco Cuturi. The Monge gap: A regularizer to learn all transport maps. *arXiv preprint arXiv:2302.04953*, 2023.
- [45] Ashish Vaswani, Noam Shazeer, Niki Parmar, Jakob Uszkoreit, Llion Jones, Aidan N Gomez, Łukasz Kaiser, and Illia Polosukhin. Attention is all you need. *Advances in neural information processing systems*, 30, 2017.
- [46] Pauli Virtanen, Ralf Gommers, Travis E. Oliphant, Matt Haberland, Tyler Reddy, David Cournapeau, Evgeni Burovski, Pearu Peterson, Warren Weckesser, Jonathan Bright, Stéfan J. van der Walt, Matthew Brett, Joshua Wilson, K. Jarrod Millman, Nikolay Mayorov, Andrew R. J. Nelson, Eric Jones, Robert Kern, Eric Larson, C J Carey, İlhan Polat, Yu Feng, Eric W. Moore, Jake VanderPlas, Denis Laxalde, Josef Perktold, Robert Cimrman, Ian Henriksen, E. A. Quintero, Charles R. Harris, Anne M. Archibald, Antônio H. Ribeiro, Fabian Pedregosa, Paul van Mulbregt, and SciPy 1.0 Contributors. *SciPy 1.0: Fundamental Algorithms for Scientific Computing in Python*, 2020.
- [47] Ling Yang, Zhilong Zhang, Yang Song, Shenda Hong, Runsheng Xu, Yue Zhao, Wentao Zhang, Bin Cui, and Ming-Hsuan Yang. Diffusion models: A comprehensive survey of methods and applications. *ACM Computing Surveys*, 2022.
- [48] Manzil Zaheer, Satwik Kottur, Siamak Ravanbakhsh, Barnabas Poczos, Russ R Salakhutdinov, and Alexander J Smola. Deep sets. *Advances in neural information processing systems*, 30, 2017.

A Eye candies

We collect the level curves of the ground-truth potentials and the ones recovered with each of our methods, together with the predictions of the particles evolution super-imposed to the ground-truth population data, in Figure 2. The plots discussed in Section 4.2 are in Figure 6.

B Details on the data generation

The prediction scheme for each particle,

$$x_{t+1} = x_t - \tau \nabla V(x_t) - \tau \int_{\mathbb{R}^d} \nabla U(x_t - y) d\mu_t(y) + \sqrt{2\tau\beta} n_t, \quad (13)$$

where n_t is sampled from the d -dimensional Gaussian distribution at each t , follows from the Euler-Maruyama discretization (see [23]) of the diffusion process

$$dX(t) = -\nabla V(X(t))dt - \int_{\mathbb{R}^d} \nabla U(X(t) - y) d\mu_t(y)dt + \sqrt{2\beta} dW(t).$$

In particular, we sample 1000 particles (in Section 4.2, we sample the number of particles described in the experiment) uniformly in $[-4, 4]^d$ and update their state according to Equation (13) for 5 timesteps, for a total of 6 snapshots including the initialization.

C Training and model details

This section describes the training details for our model JK0net*.

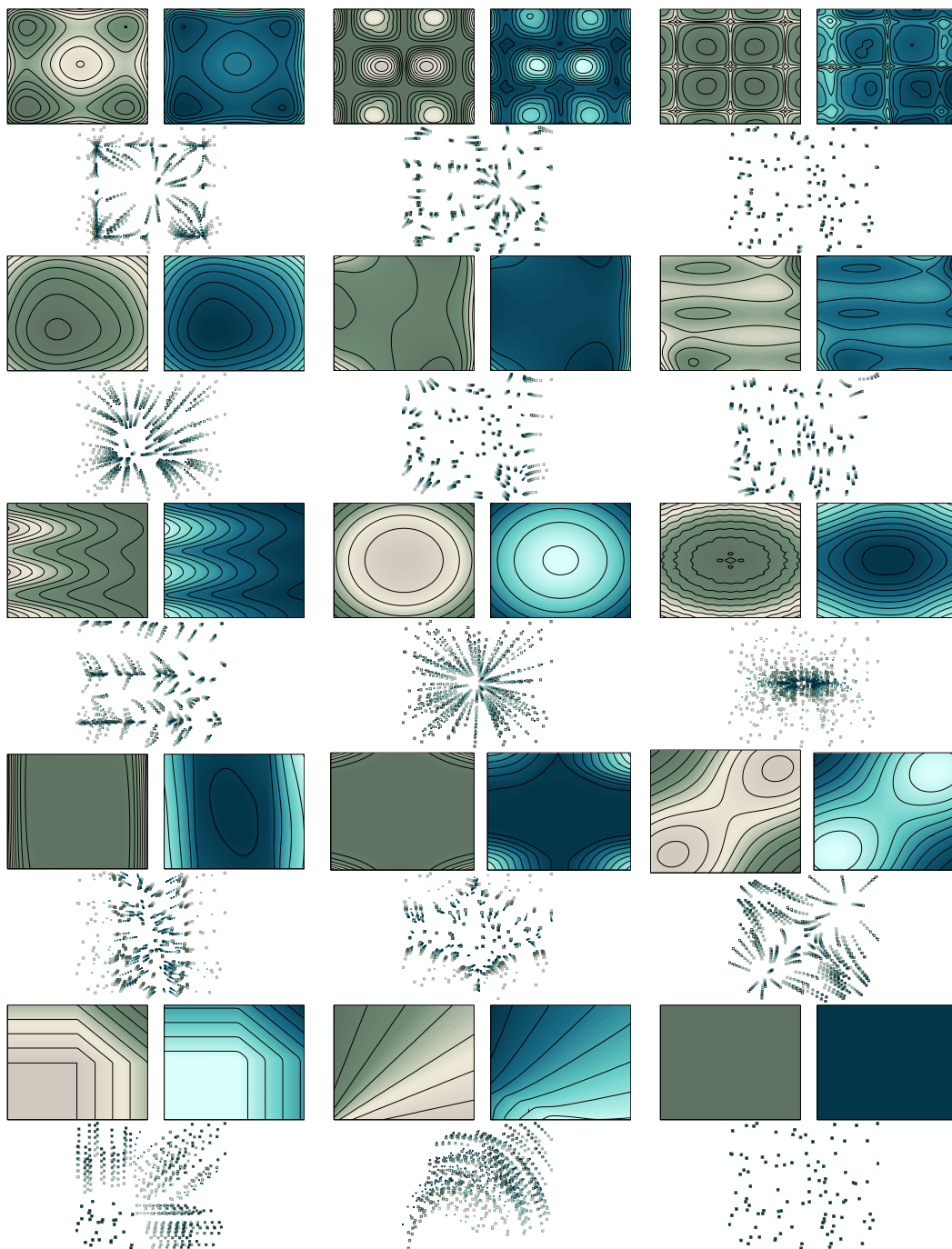


Figure 5: Level curves of the true (green-colored) and estimated (blue-colored) potentials in Appendix F, from top-left to bottom-right, row-by-row. The third plot of each group depicts the observed (empty green squares) and predicted (blue crosses) particles evolution.

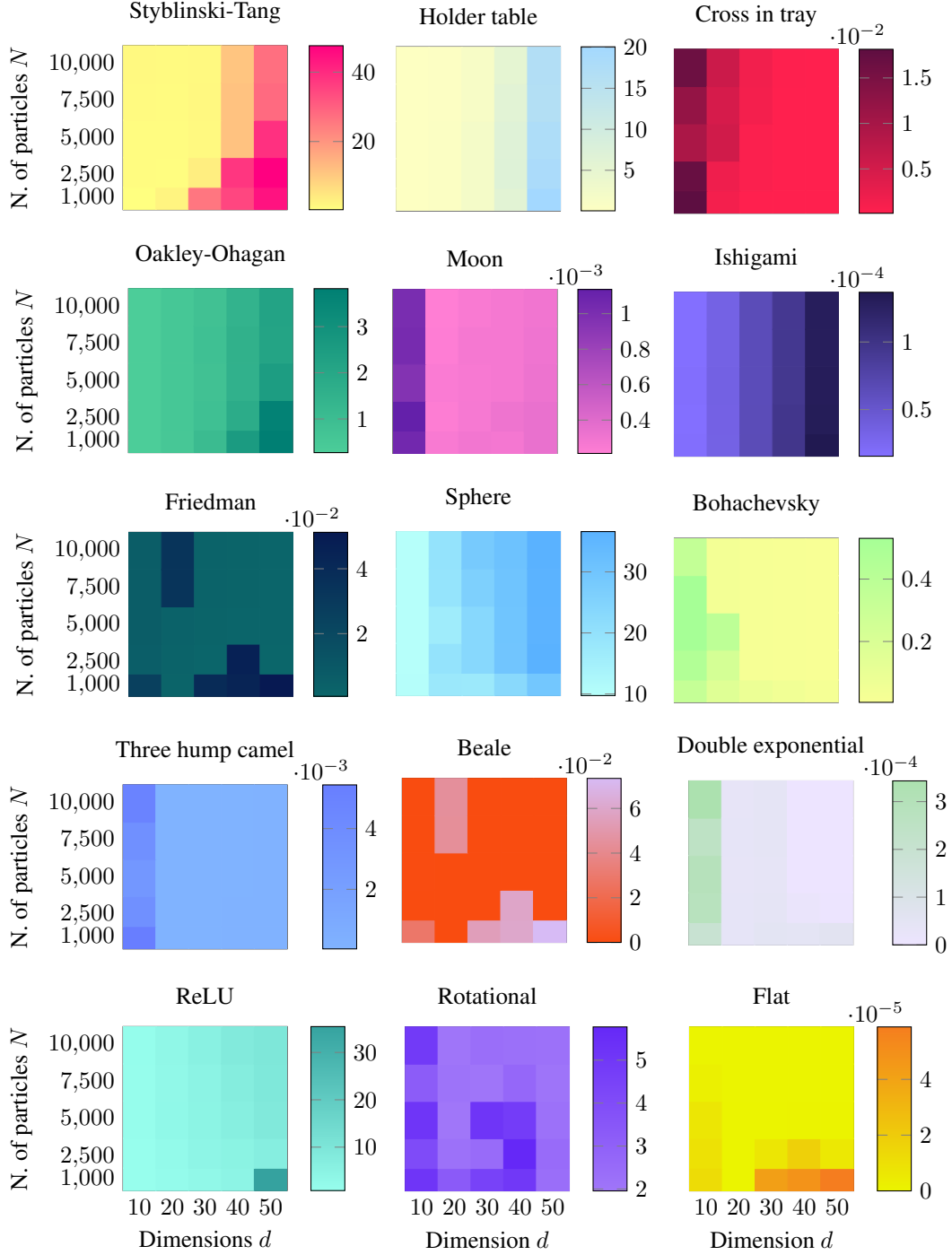


Figure 6: Additional numerical results for Section 4.2. Each heat-map corresponds to a functional in Appendix F, from top-left to bottom-right, row-by-row. The x-axis corresponds to the dimension and the y-axis to the number of particles. The colors of each cell represent the Wasserstein error. Thus, a method that scales well to high-dimensional settings should display a relatively stable color along the rows (the error is related to the norm and, thus, is linear in the dimension d ; here, the growth is sublinear).

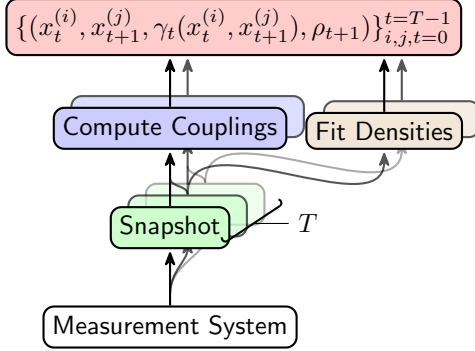


Figure 7: Data pipeline for JK0net*.

C.1 Data pre-processing

In principle, a measurement system is used to take a trajectory of populations. Then, we compute the optimal couplings between consecutive snapshots and, if needed, infer the density of each snapshot. This information is then combined to get the training set (see Figure 7). If the number of particles per snapshot is very large, one may consider splitting the single snapshot into multiple ones and computing the couplings of the sub-sampled population. For datasets larger than 1000 particles, we use a batch size of 1000.

C.2 Computation of the optimal couplings

The raw population data $\mu_0, \mu_1, \dots, \mu_T$ are typically empirical. Since they are not optimization variables in the learning task, the optimal couplings $\gamma_0, \gamma_1, \dots, \gamma_T$ can be computed beforehand for a large batch size. Differently from [8], we do not need to track the gradients within the Sinkhorn algorithm to compute the back-propagation [12], and we do not need to solve any optimal transport problem during training.

C.3 Estimation of ρ and $\nabla\rho$

The case with θ_3 non-zero imposes the estimation of the density ρ_t and its gradient $\nabla\rho_t$ from the empirical probability measures μ_t . To the extent of estimating ρ_t , there are many viable options (e.g., see the SciPy package [46]). We use a mixture of 10 gaussians for all the experiments in this paper. To compute $\nabla\rho_t$, we rely on the autograd feature of JAX [5]. The complexity related to ρ_t and $\nabla\rho_t$, instead, is bypassed if there is no internal energy in (10) (i.e., $\theta_3 = 0$).

C.4 Optimizer

We use the Adam optimizer [22] with the parameters $\beta_1 = 0.9, \beta_2 = 0.999, \varepsilon = 1e-8$, and constant learning rate $lr = 1e-3$. The model is trained with gradient clipping with maximum global norm for an update of 10. We process the data in batches of 250 particles.

C.5 Network architecture

The neural networks of potential and interaction energies are multi-layer perceptrons with 2 hidden layers of size 64 with softplus activation functions and a one-dimensional output layer (cf. [8]). Future work shall investigate different architectures for the interaction energy, for instance using (Set-)Transformers [27, 45] or Deep Sets [48].

C.6 Features selection for the linear approximation

The features used in this work are polynomials up to degree 4 and radial basis exponential functions $\exp\left(-\frac{\|v-c\|^2}{\sigma}\right)$ with $\sigma = 0.5$ and c in the discretized (10 points per dimension) grid $[-4, 4]^d$.

Finally, we use a regularizer $\lambda = 0.01$ on the square norm of the parameters $\theta = [\theta_1^\top, \theta_2^\top, \theta_3^\top]^\top$.

C.7 Hardware

The empirical evidence was entirely collected on a Macbook Pro with M2 processor.

D Proofs

D.1 Preliminaries

We briefly collect and summarizes the notation, definitions, and results of [26] used in the proofs of this work. For more intuition and details, we refer the reader to [26]. A sequence $(\mu_n)_{n \in \mathbb{N}} \subseteq \mathcal{P}(\mathbb{R}^d)$ converges narrowly to μ if $\int_{\mathbb{R}^d} \phi(x) d\mu_n(x) \rightarrow \int_{\mathbb{R}^d} \phi(x) d\mu(x)$ for all bounded continuous functions $\phi : \mathbb{R}^d \rightarrow \mathbb{R}$. We say that the convergence is ‘‘in Wasserstein’’ if $W_2(\mu_n, \mu) \rightarrow 0$ or, equivalently, $\int_{\mathbb{R}^d} \phi(x) d\mu_n(x) \rightarrow \int_{\mathbb{R}^d} \phi(x) d\mu(x)$ for all continuous functions $\phi : \mathbb{R}^d \rightarrow \mathbb{R}$ with at most quadratic growth (i.e., $\phi(x) \leq A(1 + \|x\|^2)$ for some $A > 0$). For $i, m \in \mathbb{N}, 1 \leq i \leq m$, we denote by $\pi_i : (\mathbb{R}^d)^m \rightarrow \mathbb{R}^d$ the projection map on the i^{th} component, i.e., $\pi_i(x_1, \dots, x_m) = x_i$. We compose projections as $\pi_{ij}(x) = (\pi_i(x), \pi_j(x))$.

Wasserstein calculus. We use two notions of subdifferentiability in the Wasserstein space.

- *Regular Wasserstein subdifferentiability.* A transport plan $\bar{\xi} \in \mathcal{P}(\mathbb{R}^d \times \mathbb{R}^d)$ belongs to the regular subdifferential of a functional $J : \mathcal{P}(\mathbb{R}^d) \rightarrow \mathbb{R}$ at $\bar{\mu} \in \mathcal{P}(\mathbb{R}^d)$, denoted $\hat{\partial}J(\bar{\mu})$, if for all $\mu \in \mathcal{P}(\mathbb{R}^d)$ and $\xi \in (\pi_1, \pi_2 - \pi_1)_{\#} \Gamma_0(\bar{\mu}, \mu)$ we have

$$J(\mu) - J(\bar{\mu}) \geq \max_{\substack{\alpha \in \mathcal{P}(\mathbb{R}^d \times \mathbb{R}^d \times \mathbb{R}^d) \\ \pi_{12\#} \alpha = \bar{\xi}, \pi_{13\#} \alpha = \xi}} \int_{\mathbb{R}^d \times \mathbb{R}^d \times \mathbb{R}^d} \bar{v}^\top v d\alpha(\bar{x}, \bar{v}, v) + o(W_2(\bar{\mu}, \mu)).$$

Here, α can be interpreted as a coupling of the tangent vectors $\bar{\xi}$ (the subgradient) and ξ (the tangent vector $\mu - \bar{\mu}$).

- *(General) Wasserstein subdifferentiability.* A transport plan $\bar{\xi} \in \mathcal{P}(\mathbb{R}^d \times \mathbb{R}^d)$ belongs to the (general) subdifferential of a functional $J : \mathcal{P}(\mathbb{R}^d) \rightarrow \mathbb{R}$ at $\bar{\mu}$, denoted $\partial J(\bar{\mu})$, if there are sequences $(\mu_n)_{n \in \mathbb{N}} \subset \mathcal{P}(\mathbb{R}^d)$ and $(\xi_n)_{n \in \mathbb{N}} \subset \mathcal{P}(\mathbb{R}^d \times \mathbb{R}^d)$ so that (i) $\xi_n \in \hat{\partial}J(\mu_n)$, (ii) ξ_n converges in Wasserstein to $\bar{\xi}$.

From these definitions, the analogous ones for the supergradient follows: The regular supergradients of J at $\bar{\mu}$ are the elements of $-\hat{\partial}(-J)(\bar{\mu})$ and the supergradients as the elements of $-\partial(-J)(\bar{\mu})$. We then call the *gradient* of J the unique element, if it exists, of $-\hat{\partial}(-J)(\bar{\mu}) \cap \hat{\partial}J(\bar{\mu})$, and we say that J is differentiable.

Necessary Conditions for Optimality. For J proper and lower semi-continuous w.r.t. convergence in Wasserstein (i.e., if μ_n converges in Wasserstein to μ , then $\liminf_{n \rightarrow \infty} J(\mu_n) \geq J(\mu)$), consider the optimization problem

$$\inf_{\mu \in \mathcal{P}(\mathbb{R}^d)} J(\mu). \quad (14)$$

Then, if $\mu^* \in \mathcal{P}(\mathbb{R}^d)$ is optimal for (14), i.e., $J(\mu^*) = \inf_{\mu \in \mathcal{P}(\mathbb{R}^d)} J(\mu)$, it must satisfy the ‘‘Fermat’s rule in Wasserstein space’’ (see [26, Theorem 3.3]):

$$0_{\mu^*} := \mu^* \times \delta_0 \in \partial J(\mu^*). \quad (15)$$

In particular, this implies that for some $\xi \in \partial J(\mu^*)$ it must hold

$$0 = \int_{\mathbb{R}^d \times \mathbb{R}^d} \|v\|^2 d\xi(x^*, v). \quad (16)$$

Outline of the appendix and proofs strategy Although the statement of Proposition 3.1 follows directly from Proposition 3.2, we prove it separately in Appendix D.3 as it is the simplest setting and, thus, the easiest for the reader to familiarize with the techniques used in this work. Since the internal energy (perhaps surprisingly) simplifies the setting by restricting to absolutely continuous measures (i.e., $\{\mu \in \mathcal{P}(\mathbb{R}^d) : \mu \ll dx\}$), we prove also the statement for potential and interaction energy only in Appendix D.4. We then provide the proof for the most general statement in Appendix D.5. All the proofs follow the same recipe. First, we prove existence of a solution. Second, we characterize the Wasserstein subgradients for the functional considered. Finally, we conclude deploying [26, Theorem 3.3]. Because the Wasserstein subgradients will be constructed using the subdifferential calculus rules (cf. [26, Proposition 2.17 and Corollary 2.18]), we collect them all in Appendix D.2. This appendix ends with Appendix D.6, in which we prove Proposition 3.4 using standard \mathbb{R}^d optimization arguments.

D.2 Wasserstein subgradients

(Scaled) Wasserstein distance. By [26, Corollary 2.12], the (Wasserstein) subgradients of $\frac{1}{2}W_2(\mu, \mu_t)^2$ at $\mu \in \mathcal{P}(\mathbb{R}^d)$ are all of the form $(\pi_1, \pi_1 - \pi_2)_{\#} \gamma_t$, for an optimal transport plan γ_t between μ and μ_t . Then, by [26, Corollary 2.18], the subgradients of $\frac{1}{2\tau}W_2(\mu, \mu_t)^2$ are

$$\left(\pi_1, \frac{\pi_1 - \pi_2}{\tau} \right)_{\#} \gamma_t. \quad (17)$$

Since the Wasserstein distance is in general not regularly subdifferentiable (cf. [26, Proposition 2.6]), it is not differentiable.

Potential energy. Under the assumptions in Propositions 3.1, 3.2 and 3.4, we deploy [26, Proposition 2.13] to conclude that the potential energy is differentiable at $\mu \in \mathcal{P}(\mathbb{R}^d)$ with gradient given by

$$(\text{Id}, \nabla V)_{\#} \mu. \quad (18)$$

Interaction energy. Under the assumptions in Propositions 3.2 and 3.4, we deploy [26, Proposition 2.15] to conclude that the interaction energy is differentiable at $\mu \in \mathcal{P}(\mathbb{R}^d)$ with gradient given by

$$\left(\text{Id}, \int_{\mathbb{R}^d} \nabla U(\text{Id} - x) d\mu(x) \right)_{\#} \mu. \quad (19)$$

Internal energy. Under the assumptions in Propositions 3.2 and 3.4, we deploy [25, Example 2.3] and the consistency of the tangent space (cf. [26, §2.2]) to conclude that the internal energy is differentiable at $\mu \ll dx$ with gradient given by

$$\left(\text{Id}, \frac{\nabla \rho}{\rho} \right)_{\#} \mu. \quad (20)$$

In particular, here we consider $\mu \ll dx$ since the internal energy is otherwise $+\infty$ by definition and μ is certainly not a minimum.

D.3 Proof of Proposition 3.1

The JKO step in Proposition 3.1 is the optimization problem, resembling (14),

$$\inf_{\mu \in \mathcal{P}(\mathbb{R}^d)} \left\{ J(\mu) := \int_{\mathbb{R}^d} V(x) d\mu(x) + \frac{1}{2\tau} W_2(\mu, \mu_t)^2 \right\}.$$

Since V is lower bounded, up to replacing V by $V - \min_{x \in \mathbb{R}^d} V(x)$, we can without loss of generality assume that V is non-negative. We now proceed in three steps.

Existence of a solution.

- *J has closed level sets w.r.t. narrow convergence.* As an intermediate step to prove compactness of the level sets we prove their closedness, which is equivalent to lower semi-continuity of J .

Since V is continuous and lower bounded, the functional $\mu \mapsto \int_{\mathbb{R}^d} V(x) d\mu(x)$ is lower semi-continuous [25]. The Wasserstein distance is well-known to be lower semi-continuous [26]. Thus, their sum J is also lower semi-continuous.

- J has compact (w.r.t. narrow convergence) level sets. Without loss generality, assume λ is large enough so that the level set is not empty. Otherwise, the statement is trivial. Closedness of the level sets follows directly from lower semi-continuity, thus it suffices to prove that level sets are contained in a compact set, because closed subsets of compact spaces are compact. By non-negativity of V ,

$$\begin{aligned} \{\mu \in \mathcal{P}(\mathbb{R}^d) : J(\mu) \leq \lambda\} &\subset \left\{ \mu \in \mathcal{P}(\mathbb{R}^d) : \frac{1}{2\tau} W_2(\mu, \mu_t)^2 \leq \lambda \right\} \\ &= \{\mu \in \mathcal{P}(\mathbb{R}^d) : W_2(\mu, \mu_t)^2 \leq 2\tau\lambda\}. \end{aligned}$$

Since the Wasserstein distance has compact level sets [25] w.r.t. narrow convergence, we conclude.

- *Compact level sets imply existence of a solution.* Let $\alpha := \inf_{\mu \in \mathcal{P}(\mathbb{R}^d)} J(\mu)$ and let $(\mu_n)_{n \in \mathbb{N}}$ so that $J(\mu_n) \rightarrow \alpha$. Then, by definition of convergence, $\mu_n \in \{\mu \in \mathcal{P}(\mathbb{R}^d) : J(\mu) \leq 2\alpha\}$ for all n sufficiently large. By compactness of the level sets, μ_n converges narrowly (up to subsequences) to some $\mu \in \{\mu \in \mathcal{P}(\mathbb{R}^d) : J(\mu) \leq \lambda\}$. Since compactness of the level sets implies closedness and a functional with closed level sets is lower semi-continuous (w.r.t. narrow convergence) we conclude $J(\mu) \leq \liminf_{n \rightarrow \infty} J(\mu_n) = \alpha$. Thus, μ is a minimizer of J .

Wasserstein subgradients. By [26, Proposition 2.17], we combine (17) and (18) to conclude that any subgradient of J at μ_{t+1} must be of the form $(\pi_1, \pi_2 + \pi_3)_{\#} \alpha$, for some “sum” coupling $\alpha \in \mathcal{P}(\mathbb{R}^d \times \mathbb{R}^d \times \mathbb{R}^d)$, $\pi_{12\#} \alpha = (\text{Id}, \nabla V)_{\#} \mu_{t+1}$ and $\pi_{13\#} \alpha = \left(\pi_1, \frac{\pi_1 - \pi_2}{\tau}\right)_{\#} \gamma'_{t+1}$ (cf. [26, Definition 2.1]), with γ'_{t+1} being an optimal transport plan between μ_{t+1} and μ_t .

Necessary condition for optimality. Any minimizer μ_{t+1} of J satisfies $0_{\mu_{t+1}} \in \partial J(\mu_{t+1})$. Thus, for μ_{t+1} to be optimal, there must exist γ'_{t+1} and α , so that (cf. (16))

$$\begin{aligned} 0 &= \int_{\mathbb{R}^d \times \mathbb{R}^d \times \mathbb{R}^d} \|v_2 + v_3\|^2 d\alpha(x_{t+1}, v_1, v_2) \\ &= \int_{\mathbb{R}^d \times \mathbb{R}^d \times \mathbb{R}^d} \|\nabla V(x_{t+1}) + v_2\|^2 d\alpha(x_{t+1}, v_1, v_2) \\ &= \int_{\mathbb{R}^d \times \mathbb{R}^d} \|\nabla V(x_{t+1}) + v_2\|^2 d((\pi_{13})_{\#} \alpha)(x_{t+1}, v_2) \\ &= \int_{\mathbb{R}^d \times \mathbb{R}^d} \|\nabla V(x_{t+1}) + v_2\|^2 d\left(\left(\pi_1, \frac{\pi_1 - \pi_2}{\tau}\right)_{\#} \gamma'_{t+1}\right)(x_{t+1}, v_2) \\ &= \int_{\mathbb{R}^d \times \mathbb{R}^d} \|\nabla V(x_{t+1}) + v_2\|^2 d\left(\left(\pi_1, \frac{\pi_1 - \pi_2}{\tau}\right)_{\#} \gamma'_{t+1}\right)(x_{t+1}, v_2) \\ &= \int_{\mathbb{R}^d \times \mathbb{R}^d} \left\| \nabla V(x_{t+1}) + \frac{x_{t+1} - x_t}{\tau} \right\|^2 d\gamma'_{t+1}(x_{t+1}, x_t). \end{aligned}$$

Finally, consider $\gamma_t = (\pi_2, \pi_1)_{\#} \gamma'_{t+1}$ to conclude.

D.4 The case of potential and interaction energies

As a preliminary step to Proposition 3.2, consider the case $\beta = 0$. The JKO step is the optimization problem, resembling (14),

$$J(\mu) := \int_{\mathbb{R}^d} V(x) d\mu(x) + \int_{\mathbb{R}^d \times \mathbb{R}^d} U(x - y) d(\mu \times \mu)(x, y) + \frac{1}{2\tau} W_2(\mu, \mu_t)^2. \quad (21)$$

Since V and U are lower bounded, up to replacing J with $J - \inf_{\mu \in \mathcal{P}(\mathbb{R}^d)} J(\mu)$, we can without loss of generality assume that J is non-negative.

Existence of a solution. Since also $\mu \mapsto \int_{\mathbb{R}^d \times \mathbb{R}^d} U(x - y) d(\mu \times \mu)(x, y)$ is lower semi-continuous w.r.t. narrow convergence [25], the proof of existence is analogous to the one in Proposition 3.1.

Wasserstein subgradients. By [26, Proposition 2.17], we combine (18) and (19) to conclude that each subgradient of the functional

$$\mu \mapsto \int_{\mathbb{R}^d} V(x) d\mu(x) + \int_{\mathbb{R}^d} \int_{\mathbb{R}^d} U(x-y) d\mu(y) d\mu(x) \quad (22)$$

at μ_{t+1} is of the form $(\pi_1, \pi_2 + \pi_3)_{\#} \alpha'$ for some coupling $\alpha' \in \mathcal{P}(\mathbb{R}^d \times \mathbb{R}^d \times \mathbb{R}^d)$ such that $\pi_{12\#} \alpha' = (\text{Id}, \nabla V)_{\#} \mu_{t+1}$ and $\pi_{13\#} \alpha' = (\text{Id}, \int_{\mathbb{R}^d} \nabla U(\text{Id}-x) d\mu_{t+1}(x))_{\#} \mu_{t+1}$. But then $\alpha' = (\text{Id}, \nabla V, \int_{\mathbb{R}^d} \nabla U(\text{Id}-x) d\mu_{t+1}(x))_{\#} \mu_{t+1}$ and (22) has the unique subgradient

$$\left(\text{Id}, \nabla V + \int_{\mathbb{R}^d} \nabla U(\text{Id}-x) d\mu_{t+1}(x) \right)_{\#} \mu_{t+1}. \quad (23)$$

Similarly, we conclude that $(\text{Id}, -(\nabla V + \int_{\mathbb{R}^d} \nabla U(\text{Id}-x) d\mu(x)))_{\#} \mu_{t+1}$ is the unique supergradient of (22) at μ and, thus, it is differentiable there. We can thus deploy again [26, Proposition 2.17] to combine (23) with (17) and conclude that the subgradients of (21) are of the form $(\pi_1, \pi_2 + \pi_3)_{\#} \alpha$, for $\alpha \in \mathcal{P}(\mathbb{R}^d \times \mathbb{R}^d \times \mathbb{R}^d)$, $\pi_{12\#} \alpha = (\text{Id}, \nabla V + \int_{\mathbb{R}^d} \nabla U(\text{Id}-x) d\mu_{t+1}(x))_{\#} \mu_{t+1}$ and $(\pi_1, \pi_2)_{\#} \alpha = (\pi_1, \frac{\pi_1 - \pi_2}{\tau})_{\#} \gamma'_{t+1}$ (cf. [26, Definition 2.1]), with γ'_{t+1} being an optimal transport plan between μ_{t+1} and μ_t .

Necessary condition for optimality. The steps are analogous to Appendix D.3. Any minimizer μ_{t+1} of J satisfies $0_{\mu_{t+1}} \in \partial J(\mu_{t+1})$. Thus, for μ_{t+1} to be optimal, there must exist γ'_{t+1} and α , so that (cf. (16))

$$\begin{aligned} 0 &= \int_{\mathbb{R}^d \times \mathbb{R}^d \times \mathbb{R}^d} \|v_2 + v_3\|^2 d\alpha(x_{t+1}, v_1, v_2) \\ &= \int_{\mathbb{R}^d \times \mathbb{R}^d \times \mathbb{R}^d} \left\| \nabla V(x_{t+1}) + \int_{\mathbb{R}^d} \nabla U(x_{t+1} - x) d\mu_{t+1}(x) + v_2 \right\|^2 d\alpha(x_{t+1}, v_1, v_2) \\ &= \int_{\mathbb{R}^d \times \mathbb{R}^d} \left\| \nabla V(x_{t+1}) + \int_{\mathbb{R}^d} \nabla U(x_{t+1} - x) d\mu_{t+1}(x) + v_2 \right\|^2 d((\pi_{13})_{\#} \alpha)(x_{t+1}, v_2) \\ &= \int_{\mathbb{R}^d \times \mathbb{R}^d} \left\| \nabla V(x_{t+1}) + \int_{\mathbb{R}^d} \nabla U(x_{t+1} - x) d\mu_{t+1}(x) + \frac{x_{t+1} - x_t}{\tau} \right\|^2 d\gamma'_{t+1}(x_{t+1}, x_t). \end{aligned}$$

Finally, consider $\gamma_t = (\pi_2, \pi_1)_{\#} \gamma'_{t+1}$ to conclude. Importantly, for $\beta = 0$ we do not need to restrict to $\mu \ll dx$ in Proposition 3.2, so that the statement holds regardless of β (see also Appendix D.5).

D.5 Proof of Proposition 3.2

For $\beta = 0$, see Appendix D.4. Let $\beta > 0$ here. The JKO step in Proposition 3.1 is the optimization problem, resembling (14),

$$J(\mu) := \begin{cases} \int_{\mathbb{R}^d} V(x) d\mu(x) + \int_{\mathbb{R}^d \times \mathbb{R}^d} U(x-y) d(\mu \times \mu)(x, y) \\ \quad + \beta \int_{\mathbb{R}^d} \rho(x) \log(x) dx + \frac{1}{2\tau} W_2(\mu, \mu_t)^2 & \text{if } \mu \ll \mathcal{L}, \\ +\infty & \text{else.} \end{cases} \quad (24)$$

Since V, U , and $\int_{\mathbb{R}^d} \rho(x) \log(x) dx$ are lower bounded, up to replacing J with $J - \inf_{\mu \in \mathcal{P}(\mathbb{R}^d)} J(\mu)$, we can without loss of generality assume that J is non-negative.

Existence of a solution. Since also $\mu \mapsto \int_{\mathbb{R}^d \times \mathbb{R}^d} U(x-y) d(\mu \times \mu)(x, y)$ and

$$\mu \mapsto \begin{cases} \int_{\mathbb{R}^d} \rho(x) \log(x) dx & \text{if } \mu \ll \mathcal{L}, \\ +\infty & \text{else.} \end{cases}$$

are lower semi-continuous w.r.t. narrow convergence [25], the proof of existence is analogous to the one in Proposition 3.1.

Wasserstein subgradients. When $\beta > 0$, only $\mu_{t+1} \ll \text{d}\mathcal{L}$ can be optimal and we are thus interested in characterizing the subgradients of (24) only at these probability measures. Let ρ_{t+1} be the density of μ_{t+1} . Consider first the functional

$$\mu_{t+1} \mapsto \int_{\mathbb{R}^d} V(x) \text{d}\mu_{t+1}(x) + \int_{\mathbb{R}^d} \int_{\mathbb{R}^d} U(x-y) \text{d}\mu_{t+1}(y) \text{d}\mu_{t+1}(x) + \beta \int_{\mathbb{R}^d} \rho_{t+1}(x) \log(\rho_{t+1}(x)) \text{d}x. \quad (25)$$

By [26, Proposition 2.17], we combine (23) and (20) to conclude that each subgradient of the functional (25) at μ_{t+1} is of the form $(\pi_1, \pi_2 + \pi_3)_{\#} \alpha'$ for some coupling $\alpha' \in \mathcal{P}(\mathbb{R}^d \times \mathbb{R}^d \times \mathbb{R}^d)$ such that $\pi_{12\#} \alpha' = (\text{Id}, \nabla V + \int_{\mathbb{R}^d} \nabla U(\text{Id} - x) \text{d}\mu_{t+1}(x))_{\#} \mu_{t+1}$ and $\pi_{13\#} \alpha' = (\text{Id}, \beta \frac{\nabla \rho_{t+1}}{\rho_{t+1}})_{\#} \mu_{t+1}$. But then $\alpha' = (\text{Id}, \nabla V + \int_{\mathbb{R}^d} \nabla U(\text{Id} - x) \text{d}\mu_{t+1}(x), \beta \frac{\nabla \rho_{t+1}}{\rho_{t+1}})_{\#} \mu_{t+1}$ and (22) has the unique subgradient

$$\left(\text{Id}, \nabla V + \int_{\mathbb{R}^d} \nabla U(\text{Id} - x) \text{d}\mu_{t+1}(x) + \beta \frac{\nabla \rho_{t+1}}{\rho_{t+1}} \right)_{\#} \mu_{t+1}. \quad (26)$$

Similarly, we conclude that $(\text{Id}, -(\nabla V + \int_{\mathbb{R}^d} \nabla U(\text{Id} - x) \text{d}\mu_{t+1}(x) + \beta \frac{\nabla \rho_{t+1}}{\rho_{t+1}}))_{\#} \mu_{t+1}$ is the unique supergradient of (22) at μ and, thus, it is differentiable there. We can thus deploy again [26, Proposition 2.17] to combine (26) with (17) and conclude that the subgradients of (21) are of the form $(\pi_1, \pi_2 + \pi_3)_{\#} \alpha$, for $\alpha \in \mathcal{P}(\mathbb{R}^d \times \mathbb{R}^d \times \mathbb{R}^d)$, $\pi_{12\#} \alpha = (\text{Id}, \nabla V + \int_{\mathbb{R}^d} \nabla U(\text{Id} - x) \text{d}\mu_{t+1}(x) + \beta \frac{\nabla \rho_{t+1}}{\rho_{t+1}})_{\#} \mu_{t+1}$ and $(\pi_1, \pi_2)_{\#} \alpha = (\pi_1, \frac{\pi_1 - \pi_2}{\tau})_{\#} \gamma'_{t+1}$ (cf. [26, Definition 2.1]), with γ'_{t+1} being an optimal transport plan between μ_{t+1} and μ_t .

Necessary condition for optimality. The steps are analogous to Appendices D.3 and D.4. Any minimizer μ_{t+1} of J satisfies $0_{\mu_{t+1}} \in \partial J(\mu_{t+1})$. Thus, for μ_{t+1} to be optimal, there must exist γ'_{t+1} and α , so that (cf. (16))

$$\begin{aligned} 0 &= \int_{\mathbb{R}^d \times \mathbb{R}^d \times \mathbb{R}^d} \|v_2 + v_3\|^2 \text{d}\alpha(x_{t+1}, v_1, v_2) \\ &= \int_{\mathbb{R}^d \times \mathbb{R}^d \times \mathbb{R}^d} \left\| \nabla V(x_{t+1}) + \int_{\mathbb{R}^d} \nabla U(x_{t+1} - x) + \beta \frac{\nabla \rho_{t+1}(x)}{\rho_t(x)} \text{d}\mu_{t+1}(x) + v_2 \right\|^2 \text{d}\alpha(x_{t+1}, v_1, v_2) \\ &= \int_{\mathbb{R}^d \times \mathbb{R}^d} \left\| \nabla V(x_{t+1}) + \int_{\mathbb{R}^d} \nabla U(x_{t+1} - x) + \beta \frac{\nabla \rho_{t+1}(x)}{\rho_t(x)} \text{d}\mu_{t+1}(x) + v_2 \right\|^2 \text{d}((\pi_{13})_{\#} \alpha)(x_{t+1}, v_2) \\ &= \int_{\mathbb{R}^d \times \mathbb{R}^d} \left\| \nabla V(x_{t+1}) + \int_{\mathbb{R}^d} \nabla U(x_{t+1} - x) \text{d}\mu_{t+1}(x) + \beta \frac{\nabla \rho_{t+1}(x)}{\rho_t(x)} + \frac{x_{t+1} - x_t}{\tau} \right\|^2 \text{d}\gamma'_{t+1}(x_{t+1}, x_t). \end{aligned}$$

Finally, consider $\gamma_t = (\pi_2, \pi_1)_{\#} \gamma'_{t+1}$ to conclude.

D.6 Proof of Proposition 3.4

We start with an explicit expression for the loss (11) in the case of linearly parametrized functionals:

$$\begin{aligned} \mathcal{L}(\theta_1, \theta_2, \theta_3) &:= \frac{1}{2} \sum_{t=0}^{T-1} \int_{\mathbb{R}^d \times \mathbb{R}^d} \left\| \nabla \phi_1(x_{t+1})^\top \theta_1 + \left(\int_{\mathbb{R}^d} \nabla \phi_2(x_{t+1} - x'_{t+1})^\top \text{d}\mu_{t+1}(x'_{t+1}) \right) \theta_2 \right. \\ &\quad \left. + \theta_3 \frac{\nabla \rho_{t+1}(x_{t+1})}{\rho_{t+1}(x_{t+1})} + \frac{1}{\tau} (x_{t+1} - x_t) \right\|^2 \text{d}\gamma_t(x_t, x_{t+1}). \end{aligned}$$

Since J is convex and quadratic in θ , we can find its minimum by setting the gradient to 0. In particular, the derivative of \mathcal{L} w.r.t. $\theta_1, \nabla_{\theta_1} \mathcal{L}(\theta_1, \theta_2, \theta_3)$, reads

$$\begin{aligned} \sum_{t=0}^{T-1} \int_{\mathbb{R}^d \times \mathbb{R}^d} \nabla \phi_1(x_{t+1}) & \left(\nabla \phi_1(x_{t+1})^\top \theta_1 + \left(\int_{\mathbb{R}^d} \nabla \phi_2(x_{t+1} - x'_{t+1})^\top d\mu_{t+1}(x'_{t+1}) \right) \theta_2 \right. \\ & \left. + \theta_3 \frac{\nabla \rho_{t+1}(x_{t+1})}{\rho_{t+1}(x_{t+1})} + \frac{1}{\tau} (x_{t+1} - x_t) \right) d\gamma_t(x_t, x_{t+1}). \\ & = \sum_{t=0}^{T-1} \int_{\mathbb{R}^d \times \mathbb{R}^d} \nabla \phi_1(x_{t+1}) y_{t+1}(x_{t+1})^\top \theta + \frac{1}{\tau} (x_{t+1} - x_t) d\gamma_t(x_t, x_{t+1}), \end{aligned}$$

where we used Leibniz integral rule to interchange gradient and integral. Similarly,

$$\begin{aligned} \nabla_{\theta_2} \mathcal{L}(\theta) & = \sum_{t=0}^{T-1} \int_{\mathbb{R}^d \times \mathbb{R}^d} \left(\int_{\mathbb{R}^d} \nabla \phi_2(x_{t+1} - x'_{t+1}) d\mu_{t+1}(x'_{t+1}) \right) y_{t+1}(x_{t+1})^\top \theta \\ & \quad + \frac{1}{\tau} (x_{t+1} - x_t) d\gamma_t(x_t, x_{t+1}) \\ \nabla_{\theta_3} \mathcal{L}(\theta) & = \sum_{t=0}^{T-1} \int_{\mathbb{R}^d \times \mathbb{R}^d} \frac{\nabla \rho_{t+1}(x_{t+1})^\top}{\rho_{t+1}(x_{t+1})} y_{t+1}(x_{t+1})^\top \theta + \frac{1}{\tau} (x_{t+1} - x_t) d\gamma_t(x_t, x_{t+1}). \end{aligned}$$

We split integrals and sums to get

$$\begin{aligned} \nabla_{\theta_1} \mathcal{L}(\theta) & = \left(\sum_{t=0}^{T-1} \int_{\mathbb{R}^d} \nabla \phi_1(x_{t+1}) y_t(x_{t+1})^\top d\mu_{t+1}(x_{t+1}) \right) \theta \\ & \quad + \left(\sum_{t=0}^{T-1} \int_{\mathbb{R}^d \times \mathbb{R}^d} \frac{1}{\tau} \nabla \phi_1(x_{t+1}) (x_{t+1} - x_t) d\gamma_t(x_t, x_{t+1}) \right) \\ \nabla_{\theta_2} \mathcal{L}(\theta) & = \left(\sum_{t=0}^{T-1} \int_{\mathbb{R}^d} \left(\int_{\mathbb{R}^d} \nabla \phi_2(x_{t+1} - x'_{t+1}) d\mu_{t+1}(x'_{t+1}) \right) y_t(x_{t+1})^\top d\mu_{t+1}(x_{t+1}) \right) \theta \\ & \quad + \left(\sum_{t=0}^{T-1} \int_{\mathbb{R}^d \times \mathbb{R}^d} \frac{1}{\tau} \left(\int_{\mathbb{R}^d} \nabla \phi_2(x_{t+1} - x'_{t+1}) d\mu_{t+1}(x'_{t+1}) \right) (x_{t+1} - x_t) d\gamma_t(x_t, x_{t+1}) \right) \\ \nabla_{\theta_3} \mathcal{L}(\theta) & = \left(\sum_{t=0}^{T-1} \int_{\mathbb{R}^d} \frac{\nabla \rho_{t+1}(x_{t+1})^\top}{\rho_{t+1}(x_{t+1})} y_t(x_{t+1})^\top d\mu_{t+1}(x_{t+1}) \right) \theta \\ & \quad + \left(\sum_{t=0}^{T-1} \int_{\mathbb{R}^d \times \mathbb{R}^d} \frac{1}{\tau} \frac{\nabla \rho_{t+1}(x_{t+1})^\top}{\rho_{t+1}(x_{t+1})} (x_{t+1} - x_t) d\gamma_t(x_t, x_{t+1}) \right). \end{aligned}$$

We stack these expressions to compactly write the gradient of \mathcal{L}

$$\begin{aligned} \nabla_{\theta} \mathcal{L}(\theta) & = \left(\sum_{t=0}^{T-1} \int_{\mathbb{R}^d} y_t(x_{t+1}) y_t(x_{t+1})^\top d\mu_{t+1}(x_{t+1}) \right) \theta \\ & \quad + \frac{1}{\tau} \sum_{t=0}^{T-1} \int_{\mathbb{R}^d \times \mathbb{R}^d} y_t(x_{t+1}) (x_{t+1} - x_t) d\gamma_t(x_t, x_{t+1}). \end{aligned}$$

The expression for θ follows solving $\nabla_{\theta} \mathcal{L}(\theta) = 0$ (and shifting the indices in the first sums from t to t' with $t' = t + 1$).

E Baselines settings

JK0net. We use the default configuration provided in [8]. Specifically:

- The potential energy is parametrized and optimized in the same way as for JK0net* (cf. Appendices C.4 and C.5).
- The optimal transport map is parametrized with an ICNN with two layers of 64 neurons each, with positive weights and gaussian initialization. The optimization of the transport map is performed with the Adam optimizer [22] with learning rate $lr = 0.01$, $\beta_1 = 0.5$, $\beta_2 = 0.9$ and $\varepsilon = 1e - 8$. The transport map is optimized with 100 iterations (i.e., we do not use the fixed point approach).
- We train the model for 1000 epochs in batch sizes (number of particles per snapshot) of 250, without teacher forcing and without any convex regularization. The Sinkhorn algorithm was run with $\varepsilon = 1$.

JK0net vanilla. The only difference between this method and JK0net is that we replace the ICNN with a vanilla MLP with two layers of 64 neurons each as parametrization of the optimal transport map.

JK0net with Monge Gap. The settings are the same as the vanilla JK0net, with the Monge gap [44] as additional term in the loss function for the optimal transport map (inner loop). For the computation of the Monge gap we used the recommended implementation in [44], namely the one in the OTT-JAX package [12]. The coefficient of the Monge gap regularization was set to 1.0. No results are reported on the performance of this method because the computational effort experienced rendered the results not interesting a priori (they were on par with JK0net, but the time required per experiment is orders of magnitude more).

F Functionals

We tested our methods on a selection of functionals from standard optimization tests [41]. We report the functionals used with (a projection of) their level set (see Figure 2) for completeness and reproducibility. For $v \in \mathbb{R}^d$, we conveniently define

$$z_1 := \frac{1}{\lfloor d/2 \rfloor} \sum_{i=1}^{\lfloor d/2 \rfloor} v_i \quad \text{and} \quad z_2 := \frac{1}{d - \lfloor d/2 \rfloor} \sum_{i=\lfloor d/2 \rfloor+1}^d v_i$$

to extend some 2D functions to multiple dimensions.

Styblinski-Tang

$$0.5 \sum_{i=1}^d (v_i^4 - 16v_i^2 + 5v_i) \tag{27}$$

Holder table

$$10 \left| \sin(z_1) \cos(z_2) \exp \left(\left| 1 - \frac{\|v\|}{\pi} \right| \right) \right| \tag{28}$$

Cross in tray

$$-2 \left(\left| \sin(z_1) \sin(z_2) \exp \left(\left| 10 - \frac{\|v\|}{\pi} \right| \right) \right| + 1 \right)^{0.1} \tag{29}$$

Oakley-Ohagan

$$5 \sum_{i=1}^d (\sin(v_i) + \cos(v_i) + v_i^2 + v_i) \tag{30}$$

Moon

$$\min(\max(v^\top M v, 100), -100), \tag{31}$$

with $M \in \mathbb{R}^{21 \times 21}$ defined as

$$M := \begin{bmatrix} 0 & \dots & 0 & & & & & & & & \\ -2.08 & 1.42 & 0 & \dots & 0 & & & & & & \\ 2.11 & 2.18 & -1.70 & \dots & 0 & & & & & & \\ 0.76 & 0.58 & 0.84 & 1.00 & 0 & \dots & 0 & & & & \\ -0.57 & -1.21 & 1.20 & -0.49 & -3.23 & \dots & 0 & & & & \\ -0.72 & -7.15 & -2.35 & 1.74 & 2.75 & -1.10 & \dots & 0 & & & \\ -0.47 & -1.29 & -0.16 & 1.29 & -1.40 & 2.34 & 0.21 & 0 & \dots & 0 & \\ 0.39 & -0.19 & -0.35 & 0.24 & -3.90 & -0.03 & -4.16 & 0 & \dots & 0 & \\ 1.40 & -2.75 & -5.93 & -4.73 & -0.70 & -0.80 & -0.37 & 0.26 & -1.00 & 0 & \\ 0 & \dots & 0 & & & & & & & & \\ -0.09 & -1.16 & -1.15 & 3.27 & -0.17 & 0.13 & -1.27 & -0.30 & 0.77 & 3.06 & \\ 0 & \dots & 0 & & & & & & & & \\ -0.7 & -1.09 & 1.89 & 1.87 & -3.38 & -3.97 & 2.78 & -2.69 & 1.09 & 2.46 & \\ 3.34 & 0 & \dots & 0 & & & & & & & \\ -1.27 & 0.89 & -3.47 & 1.42 & -1.87 & 1.99 & 1.37 & -2.56 & -1.15 & 5.80 & \\ 2.36 & 0 & \dots & 0 & & & & & & & \\ -1.03 & -0.16 & -0.07 & -0.96 & -0.17 & 0.45 & -2.75 & 28.99 & -1.09 & -5.15 & \\ -1.77 & 0 & \dots & 0 & & & & & & & \\ 1.07 & 4.43 & 0.60 & -0.91 & 1.56 & 1.77 & -3.15 & -2.13 & -2.74 & -2.05 & \\ -3.16 & 0 & \dots & 0 & & & & & & & \\ & & & & & & & & & & \\ 2.23 & 1.65 & -1.09 & 2.06 & 2.40 & -0.50 & 1.86 & 1.36 & 1.59 & 3.17 & \\ 1.89 & 0 & \dots & 0 & & & & & & & \\ -1.31 & -1.35 & 0.44 & 0.25 & 0.32 & 0.02 & -0.74 & 3.09 & 0.48 & -0.49 & \\ -0.71 & 0 & \dots & 0 & & & & & & & \\ -2.94 & 1.15 & 1.24 & 1.97 & 2.11 & -2.08 & 1.06 & -1.73 & 2.16 & -6.71 & \\ -3.78 & 0 & \dots & 0 & & & & & & & \\ 2.63 & -19.71 & 2.13 & 3.04 & -0.20 & 1.78 & -3.76 & -1.66 & 0.34 & -0.74 & \\ 0.98 & 0 & \dots & 0 & & & & & & & \\ 0.07 & 23.72 & -0.71 & 2.00 & 1.39 & 1.76 & -0.43 & -3.94 & 4.17 & 2.78 & \\ 1.40 & 0 & \dots & 0 & & & & & & & \\ 2.44 & 1.42 & 1.64 & 1.64 & -2.01 & 1.30 & 1.25 & -2.56 & 0.73 & -0.41 & \\ -0.59 & 0 & \dots & 0 & & & & & & & \end{bmatrix}$$

Ishigami

$$\sin(z_1) + 7 \sin(z_2)^2 + 0.1 \left(\frac{z_1 + z_2}{2} \right)^4 \sin(z_1) \quad (32)$$

Friedman

$$\frac{1}{100} \left(10 \sin(2\pi(z_1 - 7)(z_2 - 7)) + 20 \left(2(z_1 - 7) \sin(z_2 - 7) - \frac{1}{2} \right)^2 + 10(2(z_1 - 7) \cos(z_2 - 7) - 1)^2 + \frac{1}{10}(z_2 - 7) \sin(2(z_1 - 7)) \right) \quad (33)$$

Sphere

$$-10 \|x\|^2 \quad (34)$$

Bohachevsky

$$10(z_1^2 + 2z_2^2 - 0.3 \cos(3\pi z_1) - 0.4 \cos(4\pi z_2)) \quad (35)$$

Three hump camel

$$2z_1^2 - 1.05z_1^4 + \frac{z_1^6}{6} + z_1z_2 + z_2^2 \quad (36)$$

Beale

$$\frac{1}{100} ((1.5 - z_1 + z_1z_2)^2 + (2.25 - z_1 + z_1z_2)^2 + (2.625 - z_1 + z_1z_2^3)^2) \quad (37)$$

Double exponential with $\sigma = 20$, $m = 3$, and $\mathbf{1}$ being the d -dimensional vector of ones,

$$200 \exp\left(-\frac{\|v - m\mathbf{1}\|^2}{\sigma}\right) + \exp\left(-\frac{\|v + m\mathbf{1}\|}{s}\right) \quad (38)$$

ReLU dimension: any

$$-50 \sum_{i=1}^d \max(0, v_i) \quad (39)$$

Rotational

$$10\text{ReLU}(\arctan 2(z_2 + 5, z_1 + 5) + \pi) \quad (40)$$

Flat dimension: any

$$0 \quad (41)$$